Taylor & Francis
Taylor & Francis Group

Combustion Theory and Modelling

ISSN: 1364-7830 (Print) 1741-3559 (Online) Journal homepage: http://www.tandfonline.com/loi/tctm20

Multipoint radiation induced ignition of dust explosions: turbulent clustering of particles and increased transparency

Michael A. Liberman, Nathan Kleeorin, Igor Rogachevskii & Nils Erland L. Haugen

To cite this article: Michael A. Liberman, Nathan Kleeorin, Igor Rogachevskii & Nils Erland L. Haugen (2018) Multipoint radiation induced ignition of dust explosions: turbulent clustering of particles and increased transparency, Combustion Theory and Modelling, 22:6, 1084-1102, DOI: 10.1080/13647830.2018.1470334

To link to this article: https://doi.org/10.1080/13647830.2018.1470334

Published online: 01 Jun 2018.

Combustion Theory and Modelling, 2018
Vol. 22, No. 6, 1084–1102, https://doi.org/10.1080/13647830.2018.1470334

Multipoint radiation induced ignition of dust explosions: turbulent clustering of particles and increased transparency

Michael A. Liberman[a]*, Nathan Kleeorin[b,a], Igor Rogachevskii[b,a] and Nils Erland L. Haugen[c,d]

[a]*Nordita, Stockholm University and Royal Institute of Technology, Stockholm, Sweden;* [b]*Department of Mechanical Engineering, Ben-Gurion University of the Negev, Beer-Sheva, Israel;* [c]*Department of Energy and Process Engineering, Norwegian University of Science and Technology, Trondheim, Norway;* [d]*SINTEF Energy Research, Trondheim, Norway*

(*Received 13 December 2017; accepted 12 April 2018*)

Understanding the causes and mechanisms of large explosions, especially dust explosions, is essential for minimising devastating hazards in many industrial processes. It is known that unconfined dust explosions begin as primary (turbulent) deflagrations followed by a devastating secondary explosion. The secondary explosion may propagate with a speed of up to 1000 m/s producing overpressures of over 8–10 atm, which is comparable with overpressures produced in detonation. Since detonation is the only established theory that allows rapid burning producing a high pressure that can be sustained in open areas, the generally accepted view was that the mechanism explaining the high rate of combustion in dust explosions is deflagration-to-detonation transition. In the present work we propose a theoretical substantiation of an alternative mechanism explaining the origin of the secondary explosion producing high speeds of combustion and high overpressures in unconfined dust explosions. We show that the clustering of dust particles in a turbulent flow ahead of the advancing flame front gives rise to a significant increase of the thermal radiation absorption length. This effect ensures that clusters of dust particles are exposed to and heated by radiation from hot combustion products of dust explosions for a sufficiently long time to become multi-point ignition kernels in a large volume ahead of the advancing flame. The ignition times of a fuel–air mixture caused by radiatively heated clusters of particles is considerably reduced compared with the ignition time caused by an isolated particle. Radiation-induced multipoint ignitions of a large volume of fuel–air ahead of the primary flame efficiently increase the total flame area, giving rise to the secondary explosion, which results in the high rates of combustion and overpressures required to account for the observed level of overpressures and damage in unconfined dust explosions, such as for example the 2005 Buncefield explosion and several vapour cloud explosions of severity similar to that of the Buncefield incident.

Keywords: turbulent clustering of particles; dust explosions; transparency effect; radiation-induced ignition

1. Introduction

Understandingthe origin and the mechanism of dust explosions is essential for minimising the dust explosion hazard in many industrial processes. The danger of dust explosions is a permanent threat in various industries handling combustible or inert powders of fine particles [1–6].

*Corresponding author. Email: mliber@nordita.org

Methane–air systems are life-threatening mixtures, particularly in underground coal mines. Methane from coal mines initiated explosions, and the explosions are later escalated by coal dusts [7]. Experimental studies [8] show that particles increase the turbulent burning velocity because of the increase in the turbulence level by particle–turbulence interaction. In cases with smaller particle sizes and larger dust concentrations (> 50–70 g/m^3) the turbulent burning velocity increases to be considerably larger than in cases with larger particle sizes and lower dust concentration ranges. Explosions initiated by these mixtures have destroyed infrastructure in mines and have taken thousands of lives in the past. Faraday and Lyell, who in 1845 analysed [9] one of the most destructive coal mine explosions, the one in the Haswell coal mine, had been the first who pointed to the likely key role of dust particles. In the real world, the types and nature of dust explosions are diverse. Devastating dust explosions can occur in a system of the combustible or inert particles suspended in fuel–air.

Dust explosions can be either partly or fully confined (e.g. explosions of pulverised biomass plants), or unconfined. In the majority of large-scale vapour cloud explosions (VCEs) there is clear forensic evidence that a severe explosion propagated into open uncongested areas. This is a feature of all of the large vapour cloud incidents for which detailed primary evidence is available (e.g. the 2005 Buncefield fuel storage depot explosion), and several VCEs of severity, similar to that of Buncefield, that occurred during the past decade [5,6,10,11]. Unconfined dust explosions and VCEs start with a primary accidentally ignited flame in the deflagration regime. In the majority of dust explosions, the primary flame becomes turbulent due to obstacles in the flame propagation path, and this can enhance the flame propagation speed significantly.

Historically, large-scale chemical explosions that involved a fuel (methane, propane, or butane) mixed with the atmosphere were also considered as unconfined dust explosions. Admittedly, large-scale coal mine explosions share traits with large vapour cloud incidents and may be considered as either partly or almost fully unconfined dust explosions. In real explosions it is common that the pressure waves produced by the primary flame disturb dust on the ground ahead of the flame front, so a dust explosion occurs when the dust particles are entrained and dispersed in the fuel–air. However, despite considerable efforts over more than 100 years, the mechanism governing flame propagation in dust explosions that cause extremely high combustion speeds and overpressures, and which is required to be known to account for the levels of the observed damage, still remains a major unresolved issue. Currently, most prevention and safety methods rely on empirical correlations. Although the technology for preventing dust explosions has progressed considerably, recurring accidents (VCEs) in the mining industry and fuel storage facilities call for a fundamentally improved understanding of the mechanism of flame propagation and the origin of high overpressures in these explosions.

Conventional flame propagation mechanisms in the deflagration regime cannot cause the high overpressures or explain the observed level of damage, such as for example in the Buncefield incident. Since detonation is the only established theory that allows sufficiently rapid burning to be sustained in open areas, there has been a general presumption [12–14] that deflagration-to-detonation transition (DDT), following turbulent flame acceleration, is the mechanism explaining dust explosions.

Already from the early experimental studies of DDT in ducts [15–20] it was known that the flame accelerates more rapidly if it passes through an array of turbulence-generating baffles. Turbulence acts as a perturbing force, increasing the flame surface and the overall burning rate. Channels with rough walls and obstacles are often used to study DDT, since in this case the run-up distance is better controlled [21–24]. This was presumably the reason

why the first attempts to explain DDT were heavily based on the assumption that DDT might occur only if the flame becomes turbulent, and that turbulence is the primary reason for the flame acceleration. At the same time, already at the beginning of DDT studies, Ya. B. Zel'dovich [25] showed that stretching of the flame front due to interaction with a non-uniform upstream flow velocity field in the boundary layer was the main reason for flame acceleration, while turbulence played a supplementary role. Stretching of the flame front by the sheared flow is a much stronger mechanism of flame acceleration than flame front wrinkling caused by turbulence. Indeed, DDT was observed experimentally in a smooth tube for different highly reactive mixtures, e.g. hydrogen–oxygen or ethylene–oxygen [26–28].

Deflagration-to-detonation transition in unconfined systems is more problematic. The process is scale dependent, therefore investigations at laboratory scales cannot reveal this phenomenon on large scales. In recent theoretical and numerical models, a possible mechanism of DDT in truly unconfined systems has been attributed to flame acceleration induced by flame front wrinkling caused by hydrodynamic instability of the flame. [29,30]. On the other hand, numerical simulations [31] demonstrated that possible DDT in unconfined media caused by flame interactions with turbulence are feasible only for very large turbulent velocities. In general, theoretical models whose purpose was to explain possible mechanisms of DDT in unconfined systems led to a deeper understanding of the effects of shocks, turbulence, and other mechanisms of flame acceleration on creating the conditions in which DDT can occur. Nevertheless, although these studies advanced basic understanding, they posed more questions than they answered.

The possibility that DDT occurs in large explosions in industrial accidents has generally only been recognised for highly reactive fuels such as hydrogen and ethylene, and models have been validated against a range of experimental data obtained from laboratory-scale experiments. Applying such data to industrial accidents is to take the models beyond their validation range, where they cannot be used as predictive tools. In particular, in the case of Buncefield and similar VCE incidents, the extent and density of congestion are substantially less than those required for DDT. Also it should be noted that all numerical simulations conducted to understand the nature of such explosions as transition to detonation used a simplified single-step chemical model. For the first time it was shown in [27,28] for hydrogen–oxygen and recently for hydrogen/air in [32,33] that results of simulations for both the mechanism of DDT and the run-up distance are totally different when used a single-step models are used compared with when detailed chemical schemes are used.

Several severe explosions extending to the whole cloud have been investigated in the years since the Buncefield incident. Forensic evidence and detailed reviews of many such incidents have shown serious discrepancies between the presumption that the overpressures and damage caused to a variety of objects were caused by detonation and what has been observed in most VCE incidents [5,6,11]. A detailed analysis of physical damage and data available from CCTV cameras led to conclusions [6,11] that scenarios based on detonation [10,12,14] and the type of the observed damage are not consistent with what would occur in a detonation, and that 'the combustion in Buncefield was unsteady (episodic), with periods of rapid flame advance (producing high local overpressures) being punctuated by pauses. Overall the average rate of flame progress was sub-sonic ($\sim$ 150 m/s)'.

In the present article, we consider an alternative mechanism for dust explosions that can explain the origin of the secondary explosion producing high speeds of combustion and high overpressures in unconfined dust explosions due to the radiative induced ignition of a large volume ahead of the primary advancing flame.

2. Effect of radiative preheating

It was shown in [34,35] that the radiative flux emitted by hot combustion products in large dust explosions is close to blackbody radiation at stoichiometric flame temperatures (2200–2500 K) and can make a decisive contribution to the overall energy transport, structure, and velocity of flames [36]. The experimentally measured thermal radiation caused by dust explosions, and reported values of a maximum surface emissive power, are in the range 140–556 kW/m^2 [37,38]. In unconfined dust explosions, the radiative flux emitted from the advancing flame into the reactants is significantly enhanced by the increased emissivity of the large volume of burned products containing hot particles. The role of radiation in flame propagation through the particle-laden combustible gas is an important issue that has not been sufficiently examined so far.

The impact of thermal radiation emanated by the advancing flame in dust explosions can be expected to have a range of possible outcomes. Particles suspended in an initially flammable gas mixture absorb and are heated by thermal radiation. They in turn heat the surrounding gas and can enhance the flame speed and/or cause ignition of the surrounding fuel–air mixture. This effect can play an important role in large dust explosions and VCEs.

Thermal radiation emitted from the flame, propagating in a particle-laden fuel–air mixture, is absorbed and re-emitted by the particles ahead of the flame with heat being transferred from the particles to the surrounding gas by thermal conduction. It was shown in [39,40] that this radiative preheating may result in a considerably strong increase in both the temperature ahead of the flame and the flame velocity. For evenly dispersed particles, the maximum increase in the temperature of the gas mixture immediately ahead of the flame front can be estimated as [39]

$$\Delta T_p = \frac{(1 - \mathrm{e}^{-1})\,\sigma T_b^4}{U_\mathrm{f}(\rho_p\, c_\mathrm{p} + \rho_g\, c_\mathrm{v})}, \tag{1}$$

where U_f is the normal laminar flame velocity, σT_b^4 is the blackbody radiative flux, ρ_g is the mass density of the gaseous mixture, and c_p and c_v are the specific heats of particles and the gas phase, respectively.

For evenly dispersed particles, the intensity of the radiant flux decreases exponentially on a scale in the order of the radiation absorption length, $L_a = 1/\langle\kappa\rangle \approx (2\rho_p/3\rho_d)\, d_p$, where $\langle\kappa\rangle = \sigma_p\langle N\rangle$ is the mean particle absorption coefficient, $\sigma_p \approx \pi d_p^2/4$ is the absorption cross section of a particle, d_p is the particle size (diameter), $\langle N\rangle$ is the mean particle number density, ρ_p is the material density of the dust particles, and ρ_d is the spatial particle mass density. The radiation absorption length for the dust cloud mass densities, $\rho_d = 0.01$–0.05 kg/m^3 typical for dust explosions, is in the range 1–10 cm for the micron size particles $d_p = 1$–20 μm. Therefore radiation-induced ignition of the fuel–air by the radiatively heated particles is not possible in the case of evenly dispersed particles. The situation is completely different when particles are non-uniformly dispersed, for example in the form of an optically thick dust layer separated from ahead of the flame front by a gaseous gap with a sufficiently small concentration of particles in the gap. In this case, the gap between the flame and the layer is transparent to radiation, and particles in the layer are exposed to and heated by the radiation from the flame for a sufficiently long time to become ignition kernels. It was shown in [39,40] that such an optically thick layer of particles can ignite a new combustion wave in the surrounding fuel–air mixture ahead of the flame front before it is reached by the advancing flame.

The plausibility of formation of local ignition kernels ahead of the flame can play an important role in unconfined dust explosions and vapour cloud incidents. Moore and Weinberg [41] hypothesised that fibrous particles a few millimeters across can be heated and ignited sufficiently quickly by the forward radiation from hot combustion products. This in turn may lead to multi-point ignition of a gas mixture ahead of the flame front resulting efficiently in an anomalously high rate of combustion. Li and Lindstedt [42] demonstrated experimentally multipoint radiation induced ignition by dust particles trapped in a tube around obstacles and heated by radiation from an infrared laser.

However, it should be noted that, in order for a strong secondary explosion producing a high overpressure or shock wave to occur, a multi-point ignition of a large volume of fuel–air mixture ahead of the advancing flame must be ignited by the ignition kernels of particles heated by radiation from hot combustion products. This requires the penetration length of radiation, $L_{\rm eff}$, to become so large that the particles are sufficiently exposed to and heated by the radiation in a large volume even far ahead of the flame front, i.e.

$$L_{\rm eff} \gg c_{\rm s}\,\tau_{\rm ign}, \tag{2}$$

where $c_{\rm s}$ is the speed of sound in the flow ahead of the flame and $\tau_{\rm ign}$ is the timescale of fuel–air ignition by the radiatively heated ignition kernels. This means that particles well ahead of the flame front have to be exposed to thermal radiation, and heated by it for a sufficiently long time, to ignite the surrounding mixture. We will show that clustering of particles in a turbulent flow ahead of the advancing flame gives rise to a strong (up to 2–3 orders of magnitude) increase in the radiation penetration length.

3. Effect of turbulent clustering of dust particles on radiation heat transfer

In turbulent flows ahead of the primary flame, dust particles with material density much larger than the fuel–air gas density assemble in small clusters with sizes about several Kolmogorov viscous scales. Here, $\ell_\eta = \ell_0/{\rm Re}^{3/4} \approx 0.1$–$10$ mm is the Kolmogorov viscous scale and ${\rm Re} = u_0\ell_0/\nu$ is the Reynolds number based on the integral scale, ℓ_0, of turbulence and the characteristic turbulent velocity, u_0, at the integral scale. The turbulent eddies, acting as small centrifuges, push the particles to the regions between the eddies, where the pressure fluctuations are maximum and the vorticity intensity is minimum. Therefore, suspended small particles in a turbulent flow tend to assemble in clusters with much higher particle number densities than the mean particle number density. This effect, known as inertial clustering, has been investigated in a number of analytical [43–46], numerical [47,48], and experimental [49–52] studies.

Our analytical studies [53,54] and laboratory experiments [55] have shown that the particle clustering is significantly enhanced in the presence of a mean temperature gradient, so the turbulence is temperature stratified and the turbulent heat flux is not zero. This causes correlations between fluctuations of fluid temperature and velocity, and non-zero correlations between fluctuations of pressure and fluid velocity. This enhances particle clustering in the regions of maximum pressure fluctuations. As a result, the particle concentration in clusters rises by a few orders of magnitude compared with the mean concentration of evenly dispersed particles [53,54].

It is known that spatial inhomogeneities with scales larger than the wavelength of the radiation may give rise to an increase in the radiation absorption length [56–58]. The effect of an increase in radiation transmission through gas–particle mixtures caused by inertial particle clustering in non-stratified turbulence was studied using a Monte Carlo model

in different particle distributions in [59,60]. In the case of non-stratified turbulence and for relatively small Reynolds numbers, particle clustering or the increase of the radiation absorption length is not very pronounced. On the contrary, in the case of a dust explosion, there are many reasons for the formation of an inhomogeneous temperature distribution and temperature gradients in the turbulent flow produced by pressure waves ahead of the primary flame. We will show that the clustering of particles in the temperature stratified turbulence ahead of the primary flame gives rise to a strong increase of the radiation penetration length. The effect ensures that the inequality (2) is satisfied because clusters of particles even far ahead of the primary flame are exposed to and heated by the radiation from the primary flame for a sufficiently long time to become ignition kernels.

3.1. *Equation for the mean radiation intensity*

To investigate how clustering of particles affects the radiation penetration length, and how this effect depends on the turbulence parameters, we consider a turbulent flow with suspended particles exposed to a radiative flux. The radiative transfer equation for the intensity of radiation, $I(\boldsymbol{r}, \hat{\boldsymbol{s}})$, in the two-phase flow reads (see for example [61,62])

$$(\hat{\boldsymbol{s}}\cdot\nabla)\, I(\boldsymbol{r}, \hat{\boldsymbol{s}}) = -\left[\kappa_g(\boldsymbol{r}) + \kappa_p(\boldsymbol{r}) + \kappa_s(\boldsymbol{r})\right] I(\boldsymbol{r}, \hat{\boldsymbol{s}}) + \kappa_g\, I_{b,g} + \kappa_p I_{b,p} + \frac{\kappa_s}{4\pi}\int \phi(\boldsymbol{r}, \hat{\boldsymbol{s}}, \hat{\boldsymbol{s}}')\, I(\boldsymbol{r}, \hat{\boldsymbol{s}}')\, \mathrm{d}\Omega, \tag{3}$$

where $\kappa_g(\boldsymbol{r})$ and $\kappa_p(\boldsymbol{r})$ are the absorption coefficients of gas and particles, respectively, $\kappa_s(\boldsymbol{r})$ is the particle scattering coefficient, $\phi(\boldsymbol{r}, \hat{\boldsymbol{s}}, \hat{\boldsymbol{s}}')$ is the scattering phase function, $I_{b,g}(\boldsymbol{r})$ and $I_{b,p}(\boldsymbol{r})$ are the blackbody radiation intensities for gas and particles, respectively, $\boldsymbol{r}$ is the position vector, $\hat{\boldsymbol{s}} = \boldsymbol{k}/k$ is the unit vector in the direction of radiation, $\boldsymbol{k}$ is the wave vector, (k, θ, φ) are the spherical coordinates in $\boldsymbol{k}$ space, and $\mathrm{d}\Omega = \sin\theta\, \mathrm{d}\theta\, \mathrm{d}\varphi$. Taking into account that the scattering and absorption cross sections for gases in normal conditions are very small, the contribution from the gas phase is negligible in comparison with that of particles. We also take into account that, for $\pi d_p \sqrt{|\epsilon|}/\lambda_{\mathrm{rad}} \gg 1$, the scattering coefficient is negligibly small compared with the particle absorption coefficient [62], where ϵ is the dielectric permeability of the dust particles, λ_{rad} is the radiation wavelength, and d_p is the diameter of the dust particles. Therefore, Equation (3) is reduced to

$$(\hat{\boldsymbol{s}}\cdot\nabla)\, I(\boldsymbol{r}, \hat{\boldsymbol{s}}) = -\kappa(\boldsymbol{r})\,(I(\boldsymbol{r}) - I_b)\,, \tag{4}$$

where $\kappa \equiv \kappa_p(\boldsymbol{r})$ and $I_b \equiv I_{b,p}$, which depends on the local temperature, and we have omitted the subscript 'p'.

To derive the equation for the effective radiation absorption coefficient in the presence of particle clustering in a turbulent flow, we use a mean-field approach. In the framework of this approach, all quantities are decomposed into the mean and fluctuating parts: $I = \langle I\rangle + I'$, $I_b = \langle I_b\rangle + I_b'$, and $\kappa = \langle\kappa\rangle + \kappa'$. The fluctuating parts, I', I_b', κ', have zero mean values, and angular brackets denote averaging over an ensemble of fluctuations.

The radiation absorption length for evenly dispersed particles is $L_a = 1/\langle\kappa\rangle$, where $\langle\kappa\rangle = \sigma_a\langle N\rangle$ is the mean particle absorption coefficient, $\sigma_a \approx \pi d_p^2/4$, and $\langle N\rangle$ is the mean number density of evenly dispersed particles. The particle absorption coefficient is $\kappa = n\,\sigma_a$, so that the fluctuations of the absorption coefficient are $\kappa' = n'\,\sigma_a = n'\,\langle\kappa\rangle/\langle N\rangle$. Averaging Equation (4) over the ensemble of the particle number density fluctuations, we obtain the

equation for the mean irradiation intensity $\langle I(\boldsymbol{r}, \hat{\boldsymbol{s}})\rangle$:

$$(\hat{\boldsymbol{s}}\cdot\boldsymbol{\nabla})\,\langle I(\boldsymbol{r}, \hat{\boldsymbol{s}})\rangle = -\langle\kappa\rangle\,(\langle I\rangle - \langle I_b\rangle) - \langle\kappa'\,I'\rangle + \langle\kappa'\,I'_b\rangle. \tag{5}$$

Subtracting Equation (5) from Equation (4), we obtain the equation for fluctuations of I':

$$\left(\hat{\boldsymbol{s}}\cdot\boldsymbol{\nabla} + \langle\kappa\rangle + \kappa'\right) I'(\boldsymbol{r}, \hat{\boldsymbol{s}}) = I_{\text{source}}, \tag{6}$$

where $s = \boldsymbol{r}\cdot\hat{\boldsymbol{s}}$, and the source term is

$$I_{\text{source}} = -\kappa'\,(\langle I\rangle - \langle I_b\rangle) + \langle\kappa'\,I'\rangle + \left(\langle\kappa\rangle + \kappa'\right) I'_b - \langle\kappa'\,I'_b\rangle. \tag{7}$$

The solution of Equation (6) is

$$I'(\boldsymbol{r}, \hat{\boldsymbol{s}}) = \int_{-\infty}^{\infty} I_{\text{source}}\,\exp\left[-\left|\int_{s'}^{s}\left[\langle\kappa\rangle + \kappa'(s'')\right]\,\mathrm{d}s''\right|\right]\,\mathrm{d}s'. \tag{8}$$

Expanding the exponent, $\exp\left[-\int_{s'}^{s}\kappa'(s'')\,\mathrm{d}s''\right]$, in Equation (8) in Taylor series over a small parameter, $\kappa'\ell_\eta \mathrm{Sc}^{-1/2} \ll 1$, one obtains

$$\exp\left[-\int_{s'}^{s}\kappa'(s'')\,\mathrm{d}s''\right] = 1 - \int_{s'}^{s}\kappa'(s'')\,\mathrm{d}s'' + \mathrm{O}\left(\kappa'^2\right), \tag{9}$$

so that Equation (8) reads

$$I'(\boldsymbol{r}, \hat{\boldsymbol{s}}) = \int_{-\infty}^{\infty} I_{\text{source}}\,\exp\left(-\langle\kappa\rangle|s - s'|\right)\left(1 - \int_{s'}^{s}\kappa'(s'')\,\mathrm{d}s''\right)\,\mathrm{d}s' + \mathrm{O}\left(\kappa'^2\right), \tag{10}$$

where $\mathrm{Sc} = \nu/D$ is the Schmidt number, ν is the kinematic viscosity, and D is the coefficient of the Brownian diffusion of the particles. Multiplying Equation (10) by κ' and averaging over the ensemble of fluctuations, we obtain an expression for the one-point correlation function $\langle\kappa'\,I'\rangle$:

$$\begin{aligned}\langle\kappa'\,I'\rangle &\left[1 + \int_{-\infty}^{\infty}\left(\int_{s'}^{s}\langle\kappa'(s)\kappa'(s'')\rangle\,\mathrm{d}s''\right)\exp\left(-\langle\kappa\rangle|s - s'|\right)\,\mathrm{d}s'\right] \\ &= -\left(\langle I\rangle - \langle I_b\rangle\right)\int_{-\infty}^{\infty}\langle\kappa'(s)\kappa'(s')\rangle\,\exp\left(-\langle\kappa\rangle|s - s'|\right)\,\mathrm{d}s'.\end{aligned} \tag{11}$$

To derive Equation (11), we used the quasi-linear approach [63]. In the framework of this approach, we neglected in Equation (11) small third and higher moments in fluctuations of κ', due to a small parameter in the theory, $\kappa'\ell_\eta \mathrm{Sc}^{-1/2} \ll 1$. We also neglected a small correlation between the particle number density fluctuations and the gas temperature fluctuations, which implies that $\langle\kappa'\,I'_b\rangle = 0$.

Equation (11) can be rewritten as

$$\langle\kappa'\,I'\rangle = -\langle\kappa\rangle\left(\langle I\rangle - \langle I_b\rangle\right)\frac{2\beta J_1}{1 + 2\beta J_2}, \tag{12}$$

where the values J_1 and J_2 in Equation (12) are given by the integrals

$$J_1 = \int_0^\infty \Phi(Z) \exp(-\beta Z)\, \mathrm{d}Z, \tag{13}$$

$$J_2 = \beta \int_0^\infty \left(\int_0^Z \Phi(Z')\, \mathrm{d}Z' \right) \exp(-\beta Z)\, \mathrm{d}Z, \tag{14}$$

where Z=|s-s'|/ℓ_D, $\Phi(t, \boldsymbol{R}) = \langle n'(t, \boldsymbol{x})\, n'(t, \boldsymbol{x} + \boldsymbol{R})\rangle$ is the two-point correlation function of the particle number density fluctuations, $\beta = \langle\kappa\rangle\, \ell_D$ and $\ell_D = a\, \ell_\eta/\mathrm{Sc}^{1/2}$, with the numerical factor $a \gg 1$. Substituting the correlation function $\langle\kappa'\, I'\rangle$ determined by Equation (12) into Equation (5), we obtain an equation for the mean radiation intensity:

$$(\hat{\boldsymbol{s}}\cdot\nabla)\, \langle I(\boldsymbol{r}, \hat{\boldsymbol{s}})\rangle = -\kappa_{\mathrm{eff}} \Big(\langle I\rangle - \langle I_b\rangle \Big), \tag{15}$$

where the effective absorption coefficient κ_{eff}, which takes into account the particle clustering in a temperature stratified turbulence, is

$$\kappa_{\mathrm{eff}} = \langle\kappa\rangle \left(1 - \frac{2\beta J_1}{1 + 2\beta J_2} \right). \tag{16}$$

3.2. *Effect of particle clustering*

To calculate the integrals J_1 and J_2, we use the normalised two-point correlation function of the particle number density fluctuations, $\Phi(R) = \langle n'(\boldsymbol{r})\, n'(\boldsymbol{r} + \boldsymbol{R})\rangle/\langle N\rangle^2$. The two-point correlation function that accounts for particle clustering in temperature stratified turbulence was derived in [53]: $\Phi(R) = (n_{\mathrm{cl}}/\langle N\rangle)^2$ for $0 \le R \le \ell_D$ and

$$\Phi(R) = \left(\frac{n_{\mathrm{cl}}}{\langle N\rangle} \right)^2 \left(\frac{R}{\ell_D} \right)^{-\mu} \cos\left[\alpha\, \ln\left(\frac{R}{\ell_D} \right) \right] \tag{17}$$

for $\ell_D \le R \le \infty$. This correlation function determines the maximum increase of the particle number density inside a cluster, where $R = \boldsymbol{R}\cdot\hat{\boldsymbol{s}}$,

$$\mu = \frac{1}{2(1 + 3\sigma_T)} \left[3 - \sigma_T + \frac{20\sigma_v(1 + \sigma_T)}{1 + \sigma_v} \right], \tag{18}$$

$$\alpha = \frac{3\pi(1 + \sigma_T)}{(1 + 3\sigma_T)\, \ln \mathrm{Sc}}. \tag{19}$$

Here $\sigma_{_T} = \left(\sigma_{T0}^2 + \sigma_v^2\right)^{1/2}$ is the degree of compressibility of the turbulent diffusion tensor, $\sigma_{T0} = \sigma_{_T}(\mathrm{St} = 0)$, and σ_v is the degree of compressibility of the particle velocity field:

$$\sigma_v = \frac{8\mathrm{St}^2 K^2}{3(1 + b\, \mathrm{St}^2\, K^2)}, \quad K = \left[1 + \mathrm{Re} \left(\frac{L_* \nabla\langle T\rangle}{\langle T\rangle} \right)^2 \right]^{1/2}, \tag{20}$$

$\mathrm{Re} = \ell_0 u_0/\nu$ is the Reynolds number, $\langle T\rangle$ is the mean fluid temperature, the length $L_* = c_s^2 \tau_\eta^{3/2}/9\nu^{1/2}$, and a constant b determines the value of the parameter σ_v in the limit $\mathrm{St}^2 K^2 \gg 1$. To derive Equations (17)–(20), we used Equations (42)– (46) in [53] and Equations (17) and (18) in [54].

The particle inertia is characterised by the Stokes number, $\mathrm{St} = \tau_p/\tau_\eta$, where $\tau_p = m_p/(3\pi\rho\,\nu d_p)$ is the particle Stokes time, $\tau_\eta = \tau_0/\mathrm{Re}^{1/2}$ is the Kolmogorov time, and $\tau_0 = \ell_0/u_0$ and u_0 are the characteristic time and velocity at the turbulent integral scale, ℓ_0, respectively. The size of a cluster is given by $\ell_D = a\,\ell_\eta/\mathrm{Sc}^{1/2}$. The value of the numerical factor $a \approx 5$–10 corresponds to the values obtained in the laboratory experiments of [55] and the atmospheric measurements of [54,64]. The parameter b enters into the expression for the degree of compressibility of the particle velocity field, σ_v. In the limit of large temperature gradients ($\mathrm{St}^2 K^2 \gg 1$), the value $\sigma_v = 8/3b$. Since the degree of compressibility of the particle velocity field $\sigma_v \leq 1$, the coefficient $b \geq 8/3$. On the other hand, when b is very large ($b \gg 1$), $\sigma_v \to 0$, i.e. the role of stratification of turbulence or particle inertia is negligible, which implies the absence of turbulent clustering. Therefore, it is reasonable to choose the value of b in the range $5 \leq b \leq 10$. Our analysis shows that the final result for the effective radiation penetration length, L_{eff}, is not very sensitive to the particular value of b (see below).

In the analytical study of the radiative transfer, we neglect the third and higher moments in κ' in the correlation function $\langle \kappa' I'\rangle$ due to a small parameter in the theory, $\kappa' \ell_\eta \mathrm{Sc}^{-1/2} \ll 1$. Since for inertial particles $\mathrm{Sc} = \nu/D \gg 1$, this condition is satisfied. At the same time in the study of turbulent clustering of particles, we have taken into account higher moments in the particle number density fluctuations that contribute to the effective radiation penetration length. The higher moments in κ' (i.e. in fluctuations of particle number density n') are only important within the particle clusters, while outside the clusters the higher moments in κ' are much smaller than the second moments.

The growth of particle number density inside the cluster is saturated by nonlinear effects. The particle number density inside the cluster can be restricted by depletion of particles in the surrounding flow caused by their accumulation inside the cluster. It was shown in [53] that the maximum number density of particles attained inside the cluster and caused by the particle depletion effect is given by

$$\frac{n_{\mathrm{cl}}}{\langle N\rangle} = \left(1 + \frac{\mathrm{e}\,\mu}{\pi}\,\mathrm{Sc}^{\mu/2}\,\ln \mathrm{Sc}\right)^{1/2}. \tag{21}$$

Another effect that restricts the growth of the particle number density inside the cluster is related to a momentum coupling of particles and turbulent flow, when the kinetic energies of particles and turbulence become close. Numerical modelling shows that the latter effect becomes important when the mass loading parameter (the ratio of the particle spatial density inside the cluster to the fluid density) $m_p n_{\mathrm{cl}}/\rho_g \sim 1$. In Figure 1 we show the particle number density, $n_{\mathrm{cl}}/\langle N\rangle$, within the cluster normalised by the mean particle number density versus the particle diameter d_p for different temperature gradients $|\nabla\langle T\rangle| = 0$, 1/3, and 10 K/m. The inclined lines in Figure 1 are related to the first saturation mechanism due to the particle depletion effect. The horizontal line corresponds to the second saturation mechanism caused by the momentum coupling of particles and turbulent flow with the mass loading parameter $m_p n_{\mathrm{cl}}/\rho_g \approx 1/2$. In Figure 1, the following parameters (see below) have been used: $\mathrm{Re} = 10^3$, $\nu = 0.2$ cm^2/s, $\sigma_{T0} = 1/2$, and $c_s = 450$ m/s.

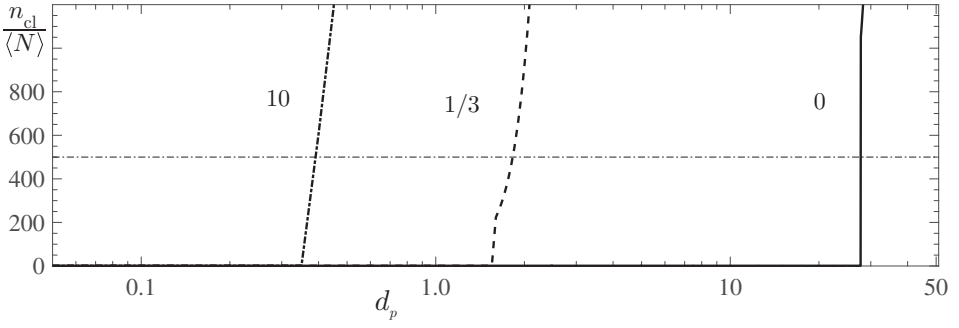

Figure 1. The particle number density, $n_{cl}/\langle N\rangle$, within the cluster normalised by the mean particle number density versus the particle diameter d_p for different temperature gradients $|\nabla\langle T\rangle| = 0$ (solid curve), 1/3 (dashed curve), and 10 K/m (dashed–dotted curve). The inclined lines are related to the first saturation mechanism due to the particle depletion effect. The horizontal line corresponds to the second saturation mechanism caused by the momentum coupling of particles and turbulent flow with the mass loading parameter $m_p n_{cl}/\rho_g \approx 1/2$.

Using Equations (17)–(20), and taking into account that $\beta = \langle\kappa\rangle\,\ell_D \ll 1$, we determine the integrals J_1 and J_2:

$$J_1 = J_2 = \left(\frac{n_{cl}}{\langle N\rangle}\right)^2 \left[1 + \frac{\mu - 1}{(\mu-1)^2 + \alpha^2}\right]. \tag{22}$$

Since the main contributions to the integrals J_1 and J_2 are from the size of the cluster, $\ell_D = a\,\ell_\eta/\mathrm{Sc}^{1/2} \propto \nu^{3/4}$, these integrals depend on the kinematic viscosity ν.

3.3. *Effective penetration length of radiation*

Substituting Equation (22) into Equation (16) for the effective absorption coefficient, we obtain the following expression for the effective penetration length of radiation, $L_{\mathrm{eff}} \equiv 1/\kappa_{\mathrm{eff}}$:

$$\frac{L_{\mathrm{eff}}}{L_a} = 1 + \frac{2a}{\mathrm{Sc}}^{1/2} \left(\frac{n_{cl}}{\langle N\rangle}\right)^2 \left(\frac{\ell_\eta}{L_a}\right) \left[1 + \frac{\mu - 1}{(\mu-1)^2 + \alpha^2}\right]. \tag{23}$$

Let us analyse the obtained result for the effect of turbulent particle clustering on the increase in the effective penetration length of radiation L_{eff}/L_a. There are two physical effects related to particle clustering that affect radiative transfer: (i) the formation of radiation transparent windows between particle clusters and (ii) the screening from the radiation of particles inside optically thick clusters. The analysis performed in the present study yields the effective absorption coefficient, κ_{eff}, which takes into account the collective effects of turbulent clusters on radiation transfer. This effect determines the formation of transparent windows between particle clusters. On the other hand, the presented analysis cannot take into account the screening effect of optically thick clusters. Therefore, the obtained results give a lower limit for the increase in the penetration length of radiation, L_{eff}, whereas the overall effect may be much stronger.

It should be noted that, following the present authors' recent article [63], Frankel *et al.* attempted in [65,66] to calculate the increase in radiation transmission through gas–particle mixtures caused by particle clustering in isothermal turbulence. However, the analytical expression for the ratio $L_{\rm eff}/L_a$ obtained in [65] differs from Equation (18) in [63] or Equation (23) in the present article. The expression for the particle radial distribution function used in [65] for the derivation of the ratio $L_{\rm eff}/L_a$ corresponds to the weak clustering regime when the clustering instability is not excited. The derivation of the ratio $L_{\rm eff}/L_a$ performed in [66] is based on the assumption of a normally-distributed optical path length. It also assumed very small particle clusters. As regards the numerical results in [65], the Reynolds numbers used (which were based on the Taylor microscale and were less than 50) imply that turbulence in this case is not fully developed, so that the increase in $L_{\rm eff}$ in comparison with the length $L_{\rm a}$ should be very small .

We first consider turbulence in the absence of the mean temperature gradient (isothermal turbulence). For isothermal turbulence, particle clustering instability occurs only when the particle diameter $d_p > 25$ μm (see [45,46,53]). Figure 2 shows the ratio $L_{\rm eff}/L_a$ versus particle size (top panel) and versus Stokes number (bottom panel) determined for the case of particle clustering in turbulence with different Reynolds numbers. The following parameters have been used for methane–air in normal conditions: $\nu = 0.2$ cm^2/s, $c_{\rm s} = 450$ m/s, $n_{\rm cl}/\langle N\rangle = 500$, and $\sigma_{T0} = 1/2$. Figure 2 demonstrates that the increase in the effective penetration length of radiation in isothermal turbulence is more than one order of magnitude for particles with $d_p > 25$ μm.

As follows from Equation (23), the ratio $L_{\rm eff}/L_a$ is strongly dependent on $(n_{\rm cl}/\langle N\rangle)^2$. Note also that, as follows from [53, Figure 1], the rate of particle cluster formation for temperature stratified turbulence is much larger (almost an order of magnitude) than that for isothermal turbulence. However, in the case of isothermal turbulence the rate of particle clustering is rather low. It is more than one order of magnitude less than the rate of particle clustering for temperature stratified turbulence (see [57, Figure 1]). Therefore, for isothermal turbulence the density of particles in clusters is unlikely to increase significantly. In this case, clusters either do not survive for a long time, or they are absorbed by the advancing flame long before the density of particles in clusters can increase significantly. It was shown in [53,54] that for temperature stratified turbulence the ratio $n_{\rm cl}/\langle N\rangle$ can increase up to three orders of magnitude.

There are many reasons for the formation of an inhomogeneity in the temperature distribution in the flow ahead of the front of the advancing flame. Therefore, it is natural to assume that in dust explosions the fluid temperature in the flow ahead of the advancing primary flame is non-uniform. As a representative example, we choose the mean temperature gradient to be in the range 0.5–3 K/m. In Figure 3, we show the ratio $L_{\rm eff}/L_a$ versus particle size (top panel) and Stokes number (bottom panel) for different values of mean temperature gradient. In this figure, the following parameters typical for turbulent flow in unconfined dust explosions have been used: ${\rm Re} = 5 \times 10^4$, $\ell_0 = 1$ m, $u_0 = 1$ m/s; $\nu = 0.2$ cm^2/s, $n_{\rm cl}/\langle N\rangle = 500$, $\sigma_{T0} = 1/2$, and $c_{\rm s} = 450$ m/s for methane–air in normal conditions. As follows from Figure 3, the increase in effective radiation penetration length for temperature stratified turbulence is much stronger than that for isothermal turbulence ($L_{\rm eff}$ increases up to three orders of magnitude compared with L_a).

4. Radiation-induced secondary explosions

In the early stage of dust explosions, an accidentally ignited sub-sonic flame accelerates due to hydrodynamic instabilities and interaction with the turbulent flow. The pressure

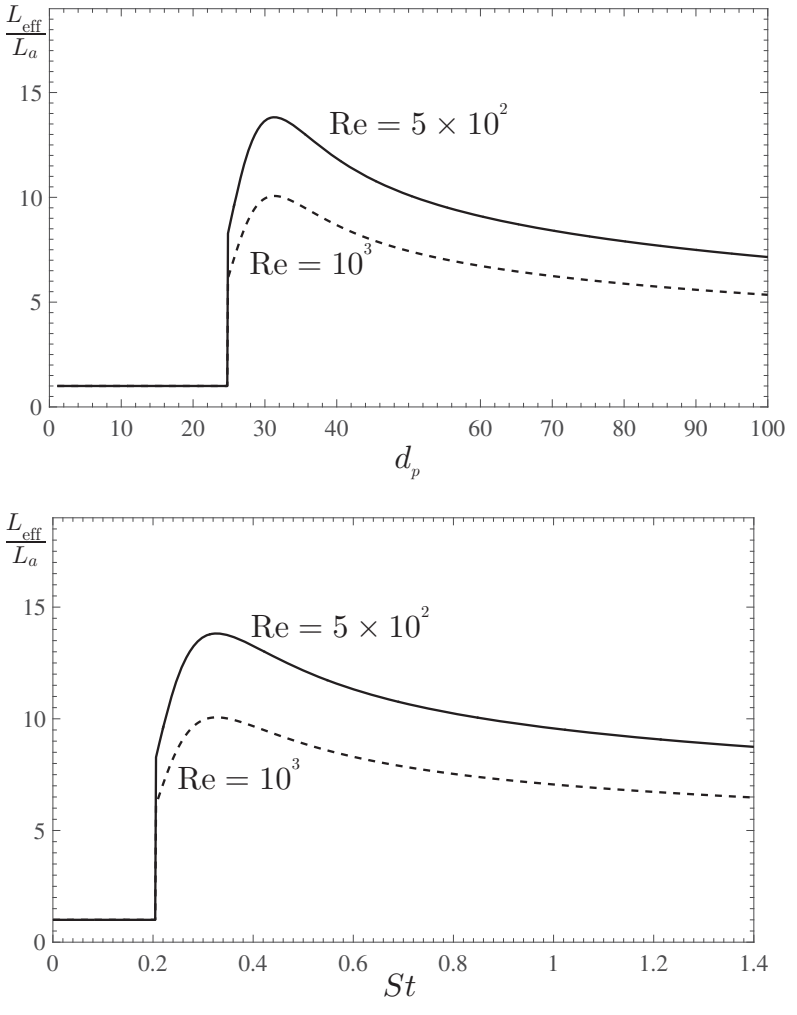

Figure 2. The ratio L_{eff}/L_a versus particle size (top panel) and Stokes number (bottom panel) for the particle clustering in isothermal turbulence with different Reynolds numbers: $\text{Re} = 5 \times 10^2$ (solid curve) and 10^3 (dashed curve).

waves produced by the accelerating flame run away and produce turbulence ahead of the advancing flame. With the increase in the primary flame surface and flame velocity, the parameters of the turbulent flow ahead of the advancing flame, i.e. Re, ℓ_0, u_0, St, and $\nabla\langle T\rangle$, change continuously. The dust particles in the turbulent flow generated assemble in clusters during a time in the order of milliseconds.

The analysis performed in the previous section shows that clustering of particles in the temperature stratified turbulent flow ahead of the primary flame may increase the radiation penetration length by up to 2–3 orders of magnitude (see Figure 4). This effect ensures that clusters of particles are exposed to and heated by the radiation from the primary flame for a sufficiently long time to become ignition kernels in a large volume ahead of the flame. The multi-point radiation-induced ignition of the surrounding fuel–air increases effectively the total flame area, so the distance, which each flame has to cover for a complete burn-out of

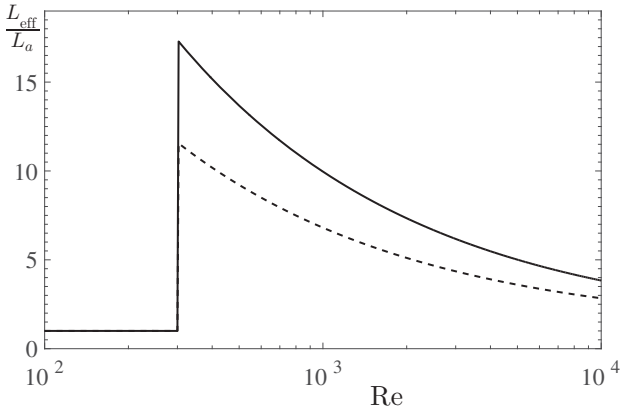

Figure 3. The ratio L_{eff}/L_a for isothermal turbulence versus the Reynolds number Re for different particle diameters: $d_p = 31.3$ (solid curve) and 40 μm (dashed curve).

the fuel, is substantially reduced. It results in a strong increase of the effective combustion speed, defined as the rate of reactant consumption of a given volume, and overpressures, required to account for the observed level of damages in unconfined dust explosions. If, for example, the radiation absorption length of evenly dispersed particles with spatial mass density 0.03 kg/m^3 was in the range of a few centimeters, dust particles assembled in the clusters of particles, are sufficiently heated by radiation at distances up to 10–20 m ahead of the advancing flame.

The experimentally measured [67,68] ignition time of the fuel–air by the radiatively heated particles is 100 ms for 10 μm non-reactive particles. The level of thermal radiation of $S \approx$ 300–400 kW/m^2, emanating from hot combustion products in dust explosions, is sufficient to raise the temperature of particles by $\Delta T_p \approx 1000$ K during $\tau_{\text{heating}} = (\rho_p\, d_p\, c_{\text{p}}\, \Delta T_p)/2S < 10$ ms. The interphase (particle–gas) energy exchange time is $\tau_{pg} = \rho_p\, d_p^2\, c_{\text{p}}/6\lambda\text{Nu} < 1$ ms, where χ is the coefficient of gas thermal conduction, and Nu ≈ 2 is the Nusselt number [67–69].

It is known that, in order for ignition to occur, a gas volume with a size that is in the order of the typical flame thickness, r_f (for CH_4/air $r_f \approx 2$ mm), has to be heated to ignition temperature to ignite self-sustained combustion in a gas mixture. This means that the time it takes for an isolated particle to heat the surrounding gas to a level where it can ignite is relatively long ($t_\chi \sim r^2/\chi \approx 500$ ms). For typical parameters in dust explosions, the Kolmogorov viscous timescale is $\tau_\eta \sim 5 \times 10^{-3}$ s, and is in the same order as the lifetime of turbulent clusters. Since the lifetime of clusters is larger than the ignition time, the theory presented in the previous section satisfactorily describes the origin and mechanism of the secondary explosion.

Numerical simulations of fuel–air ignition by a radiatively heated cluster of particles show that the ignition timescales decrease approximately as $1/n_{\text{cl}}^{1/3}$ with increasing particle number density n_{cl} in the cluster. In this case, the cluster of radiatively heated particles ignites the fuel–air mixture in a much shorter time, since the gas mixture is heated by thermal conduction within a small distance, $\Delta r = 1/n_{\text{cl}}^{1/3}$, corresponding to the particle separation in the cluster.

The above analysis indicates that the ignition time of the mixture by the radiatively heated cluster of particles is in the order of 10 ms and that the effective propagating rate of combustion caused by the secondary explosion can be estimated as $L_{\text{eff}}/\tau_{\text{ign}} \sim 10^3$ m s^{-1}.

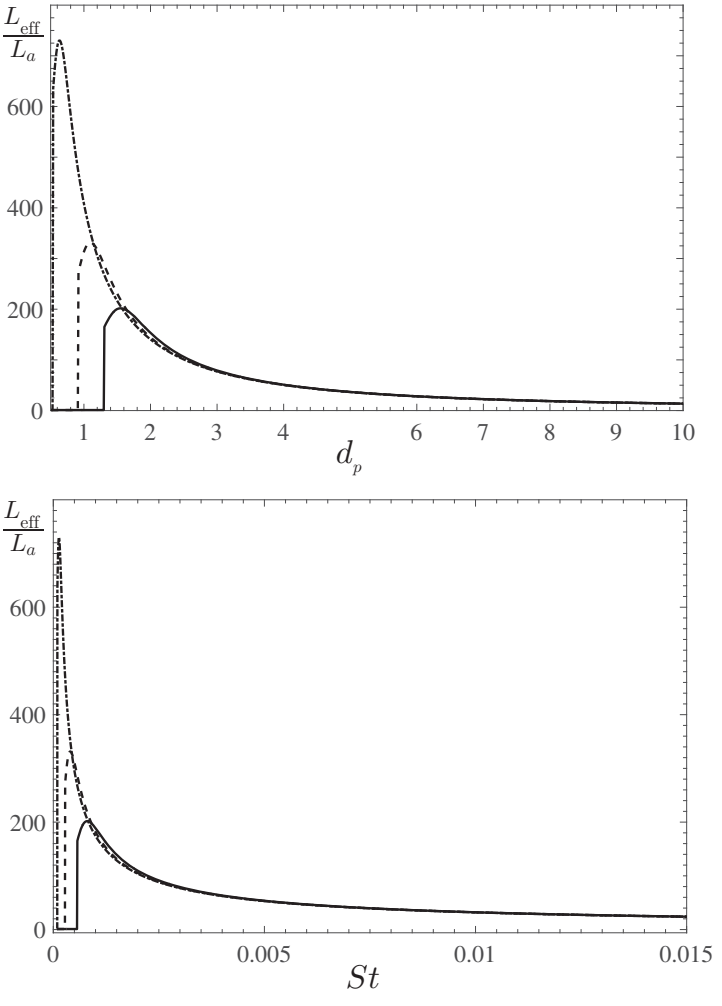

Figure 4. The ratio L_{eff}/L_a versus particle size (top panel) and Stokes number (bottom panel) for different mean temperature gradients $|\nabla\langle T\rangle| = 0.5$ (solid curve), 1 (dashed curve), and 3 K/m (dashed–dotted curve). The particle diameter is in microns.

Such a rate of the secondary explosion corresponds to the intensity of a shock wave with Mach number Ma = 2–3 producing overpressures of 8–10 atm. This may explain the mechanism of the secondary explosion and the level of damage observed in unconfined dust explosions.

Figure 5 shows the function L_{eff}/L_a versus Reynolds numbers Re calculated for particles of different diameter. It is seen that a significant increase of the radiation penetration length caused by particle clustering occurs within a rather narrow interval of turbulent parameters. The effect is much weaker if the flow parameters ahead of the flame front are changed and appear outside the 'range of transparency'. Such a dependence of L_{eff}/L_a versus Reynolds numbers suggests a possible explanation for the episodic nature of the explosion in the Buncefield incident described in [11]. For comparison, in Figure 3 we show the ratio L_{eff}/L_a

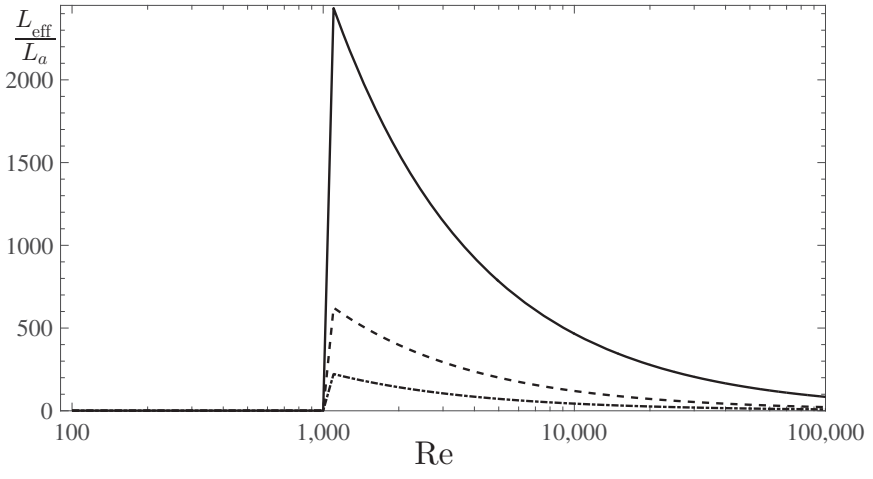

Figure 5. The ratio L_{eff}/L_a versus Reynolds number Re for different particle diameters $d_p = 1$ μm (solid curve), 5 μm (dashed curve), 10 μm (dashed–dotted curve), and for temperature gradient $|\nabla\langle T\rangle| = 3$ K/m.

versus Reynolds numbers Re for isothermal turbulence. As we mentioned before, the effect of isothermal turbulence is much weaker than that of stratified turbulence.

According to the analysis of the Buncefield explosion by Atkinson and Cusco [11]: 'The high overpressures in the cloud and low average rate of flame advance can be reconciled if the rate of flame advance was episodic, with periods of very rapid combustion being punctuated by pauses when the flame advanced very slowly. The widespread high overpressures were caused by the rapid phases of combustion; the low average speed of advance was caused by the pauses.' From the beginning, the parameters of the turbulent flow ahead of the advancing flame vary continuously and finally fall within the 'range of transparency' when the radiation penetration length increases considerably (Figures 3 and 5).

Since the primary flame is a deflagration, propagating with a velocity in the order of a few meters per second, the duration of this stage is the longest timescale in the problem. During this time the particle clusters ahead of the flame are exposed to and heated by the forward radiation for a sufficiently long time to become ignition kernels in a large volume ahead of the flame initiating the secondary explosion. Since the parameters of the turbulent flow are changed after the secondary explosion, the rapid phase of combustion is interrupted until the shock waves produced by the secondary explosion dissipate. The next phase continues until the parameters of turbulence in the flow ahead of the combustion wave fall again within the interval corresponding to the 'transparent window', such that the increased ratio L_{eff}/L_a caused by particle clustering provides conditions for the next secondary explosion.

5. Conclusions

The present study has shown that the mechanism of the secondary explosion in unconfined dust explosions and large vapour cloud explosions can be explained by the turbulent clustering of dust particles. The latter include the effect of a considerable increase in the radiation penetration length, the formation of ignition kernels in the turbulent flow caused by the primary flame, and the subsequent formation of secondary explosions, which are

caused by the impact of forward thermal radiation. The mechanism of multi-point radiation-induced ignitions due to the turbulent clustering of particles ensures that ignition of the gas mixture by the radiatively-heated clusters occurs rapidly and within a large volume ahead of the primary flame.

The described scenario of unsteady combustion consisting of rapid combustion producing high overpressures, punctuated by subsequent slow combustion, is consistent with the analysis in [11] of the Buncefield explosion. Although details of the real physical processes could be different, the proposed theoretical model describes the episodic nature of combustion in dust explosions observed in [11], and more importantly it captures the most important relevant physics. Finally, the obtained analytical solution can serve as a benchmark for numerical simulations of dust explosions, which do not need to rely on the simplifying assumptions.

The secondary explosion acts as an accelerating piston producing a strong pressure wave, which steepens into a shock wave. The intensity of the associated shock wave depends on the rate of progress of the secondary explosion and can be determined by using numerical simulations. It is possible that the condition $\tau_{\rm ign}\, c_{\rm s} \ll L_{\rm eff}$ does not hold for relatively large dust particles. Nevertheless, the increase in the effective penetration length of radiation gives rise to the secondary explosion, which propagates with the velocity $U_{\rm exp} \approx L_{\rm eff}/\tau_{\rm ign}$, which is considerably larger than the velocity of the primary flame. More detailed analysis, i.e. taking into account the particle size distribution, inter-particle collisions, possible coalescence of particles inside the clusters, and the effect of gravitational sedimentation of large particles, can only be done using numerical simulations.

Finally, it should be mentioned that transition to detonation, supported for example by forward thermal radiation in some circumstances, cannot be ruled out. It should be emphasised that the effect of a strong increase in radiation penetration length due to the turbulent clustering of particles goes beyond dust explosion applications and has many implications in astrophysical and atmospheric turbulence [54,70,71].

Acknowledgements

Helpful discussions with G. Sivashinsky, A. Mani, and participants of the NORDITA program 'Turbulent Combustion' are gratefully acknowledged.

Disclosure statement

No potential conflict of interest was reported by the authors.

Funding

The authors are grateful to the Research Council of Norway under FRINATEK [grant No. 231444] and Israel Science Foundation governed by the Israeli Academy of Sciences [grant No. 1210/15] for providing financial support for the current study. M.L. gratefully acknowledges support for this work provided by the State Key Laboratory of Explosion Science and Technology, Beijing Institute of Technology [opening project number KFJJ17-08M].

References

[1] R.K. Eckhoff, *Dust explosions in the process industries: Identification, assessment and control of dust hazards*, 3rd ed. , Gulf Professional Publishing, Houston, TX, 2003.

[2] R.K. Eckhoff, *Understanding dust explosions. The role of powder science and technology*, J. Loss Prevent. Proc. Ind. 22 (2009), pp. 105–116.

[3] T. Abbasi and S. Abbasi, *Dust explosions: Cases, causes, consequences, and control*, J. Hazard. Mater. 140 (2007), pp. 7–44.

[4] Z. Yuan, N. Khakzada, F. Khana, and P. Amyotte, *Dust explosions: A threat to the process industries*, Proc. Safety Environm. Protect. 98 (2015), pp. 57–71.
[5] G. Atkinson and J. Hall, *A review of large vapour cloud incidents*, HSL Tech. Report MH15/80, Health and Safety Executive, Harpur Hill, Buxton, UK, 2016. https://primis.phmsa.dot.gov/meetings/MtgHome.mtg?mtg=111.
[6] G. Atkinson, E. Cowpe, J. Halliday, and D. Painter, *A review of very large vapour cloud explosions: Cloud formation and explosion severity*, J. Loss Prev. Process Ind. 48 (2017), pp. 367–375.
[7] S. Kundu, J. Zanganeh, and B. Moghtaderi, *A review on understanding explosions from methane–air mixture*, J. Loss Prev. Process Ind. 40 (2016), pp. 507–523.
[8] S.R. Rockwell and A.S. Rangwala, *Influence of coal dust on premixed turbulent methane–air flames*, Combust. Flame 160 (2013), pp. 635–640.
[9] M. Faraday and C. Lyell, *Report on the explosion at the Haswell collieries, and on the means of preventing similar accidents*, London/Edinburgh/Dublin Phil. Mag. & J. Sci. (now Combust. Sci. Technol.) 26 (1845), pp. 16–35. https://doi.org/10.1080/14786444508645066.
[10] I. Herbert, *The UK Buncefield incident: The view from a UK risk assessment engineer*, J. Loss Prev. Process Ind. 23 (2010), pp. 913–920.
[11] G. Atkinson and L. Cusco, *Buncefield: A violent, episodic vapour cloud explosion*, Proc. Safety Environm. Protection 89 (2011), pp. 360–370.
[12] D. Bradley, G. Chamberlain, and D. Drysdale, *Large vapour cloud explosions, with particular reference to that at Buncefield*, Phil. Trans. R. Soc. A 370 (2012), pp. 544–566.
[13] A. Pekalski, J. Puttock, and S. Chynoweth, *Deflagration to detonation transition in a vapour cloud explosion in open but congested space: Large scale test*, J. Loss Prev. Process Ind. 36 (2015), pp. 365–370.
[14] E.S. Oran, *Understanding explosions – from catastrophic accidents to the creation of the Universe*, Proc. Combust. Inst. 35 (2015), pp. 1–35.
[15] K. Shchelkin, *Influence of the wall roughness on initiation and propagation of detonation in gases*, Zh. Eksp. Teor. Fiz. 10 (1940), pp. 823–827.
[16] K.I. Shchelkin and Y. K. Troshin, *Gasdynamics of Combustion*, Mono Book Corp., Baltimore, MD, 1965.
[17] P. Urtiew and A.K. Oppenheim, *Experimental observation of the transition to detonation in an explosive gas*, Proc. Roy. Soc. A: Math. Phys. & Engng Sci. 295 (1966), pp. 13–28. https://doi.org/10.1098/rspa.1966.0223.
[18] A. Oppenheim and R. Soloukhin, *Experiments in gasdynamics of explosions*, Annu. Rev. Fluid Mech. 5 (1973), pp. 31–58.
[19] I. Moen, M. Donato, R. Knystautas, and J. Lee, *Flame acceleration due to turbulence produced by obstacles*, Combust. Flame 39 (1980), pp. 21–32.
[20] G. Ciccarelli and S. Dorofeev, *Flame acceleration and transition to detonation in ducts*, Prog. Energy Combust. Sci. 34 (2008), pp. 499–550.
[21] A. Teodorczyk, P. Drobniak, and A. Dabkowski, *Fast turbulent deflagration and DDT of hydrogen–air mixtures in small obstructed channel*, Int. J. Hydr. Energy 34 (2009), pp. 5887–5893.
[22] G. Ciccarelli, C. Johansen, and M. Kellenberger, *High-speed flames and DDT in very rough-walled channels*, Combust. Flame 160 (2013), pp. 204–211.
[23] C. Wang, X. Dong, J. Cao, and J. Ning, *Experimental investigation of flame acceleration and deflagration-to-detonation transition characteristics using coal gas and air mixture*, Combust. Sci. Technol. 187 (2015), pp. 1805–1820.
[24] C. Wang, F. Huang, E.K. Addai, and X. Dong, *Effect of concentration and obstacles on flame velocity and overpressure of methane–air mixture*, J. Loss Prev. Process Ind. 43 (2016), pp. 302–310.
[25] Y.B. Zel'dovich, *On the theory of onset of detonation in gases*, Zh. Tekh. Fiz 17 (1947), pp. 3–26.
[26] M. Kuznetsov, V. Alekseev, I. Matsukov, and S. Dorofeev, *DDT in a smooth tube filled with a hydrogen–oxygen mixture*, Shock Waves 14 (2005), pp. 205–215. https://link.springer.com/article/10.1007/s00193-005-0265-6.
[27] M. Liberman, M. Ivanov, A. Kiverin, M. Kuznetsov, A. Chukalovsky, and T. Rakhimova, *Deflagration-to-detonation transition in highly reactive combustible mixtures*, Acta Astronautica 67 (2010), pp. 688–701.

[28] M. Ivanov, A. Kiverin, and M. Liberman, *Hydrogen–oxygen flame acceleration and transition to detonation in channels with no-slip walls for a detailed chemical reaction model*, Phys. Rev. E 83 (2011), Article ID 056313.
[29] L. Kagan and G. Sivashinsky, *Transition to detonation of an expanding spherical flame*, Combust. Flame 175 (2017), pp. 307–311.
[30] A. Koksharov, V. Bykov, L. Kagan, and G. Sivashinsky, *Transition to detonation in an unconfined space*, in: Proceedings of the 26th International Colloquium on the Dynamics of Explosions and Reactive Systems (ICDERS), 30 July–4 August 2017, Boston, MA, 2017.
[31] A.Y. Poludnenko, T.A. Gardiner, and E.S. Oran, *Spontaneous transition of turbulent flames to detonations in unconfined media*, Phys. Rev. Lett. 107 (2011), Article ID 054501.
[32] B. Rochett, F. Collin-Bastiani, L. Gicquel, O. Vermorel, D. Veynante, and T. Poinsot, *Influence of chemical schemes, numerical method and dynamic turbulent combustion modeling on LES of premixed turbulent flames*. Combust. Flame 191 (2018), pp. 417–430.
[33] O. Dounia, O. Vermorel, A. Misdariis, and T. Poinsot, *Influence of kinetics on DDT simulations* (2018), Combust. Flame, in press.
[34] G. Nathan, P. Kalt, Z. Alwahabi, B. Dally, P. Medwell, and Q. Chan, *Recent advances in the measurement of strongly radiating, turbulent reacting flows*, Prog. Energy Combust. Sci. 38 (2012), pp. 41–61.
[35] M. Hadjipanayis, F. Beyrau, R. Lindstedt, G. Atkinson, and L. Cusco, *Thermal radiation from vapour cloud explosions*, Proc. Safety Environm. Protection 94 (2015), pp. 517–527.
[36] W. Gao, T. Mogi, J. Yu, X. Yan, J. Sun, and R. Dobashi, *Flame propagation mechanisms in dust explosions*, J. Loss Prev. Process Ind. 36 (2015), pp. 186–194.
[37] P. Holbrow, S.J. Hawksworth, and A. Tyldesley, *Thermal radiation from vented dust explosions*, J. Loss Prev. Process Ind. 13 (2000), pp. 467–476.
[38] T. Roberts, A. Gosse, and S. Hawksworth, *Thermal radiation from fireballs on failure of liquefied petroleum gas storage vessels*, Proc. Safety Environm. Protection 78 (2000), pp. 184–192.
[39] M. Liberman, M. Ivanov, and A. Kiverin, *Radiation heat transfer in particle-laden gaseous flame: Flame acceleration and triggering detonation*, Acta Astronautica 115 (2015), pp. 82–93. https://doi.org/10.1016/j.actaastro.2015.05.019.
[40] M. Ivanov, A. Kiverin, and M. Liberman, *Ignition of deflagration and detonation ahead of the flame due to radiative preheating of suspended micro particles*, Combust. Flame 16 (2015), pp. 3612–3621.
[41] S. Moore and F. Weinberg, *High propagation rates of explosions in large volumes of gaseous mixtures*, Nature 290 (1981), pp. 39–40.
[42] T. Li and R. Lindstedt, *Thermal radiation induced ignition of multipoint turbulent explosions*, Proc. Safety Environm. Protection 107 (2017), pp. 108–121.
[43] T. Elperin, N. Kleeorin, and I. Rogachevskii, *Self-excitation of fluctuations of inertial particle concentration in turbulent fluid flow*, Phys. Rev. Lett. 77 (1996), pp. 5373–5376.
[44] E. Balkovsky, G. Falkovich, and A. Fouxon, *Intermittent distribution of inertial particles in turbulent flows*, Phys. Rev. Lett. 86 (2001), pp. 2790–2793.
[45] T. Elperin, N. Kleeorin, V.S. L'vov, I. Rogachevskii, and D. Sokoloff, *Clustering instability of the spatial distribution of inertial particles in turbulent flows*, Phys. Rev. E 66 (2002), Article ID 036302. https://doi.org/10.1103/PhysRevE.66.036302.
[46] T. Elperin, N. Kleeorin, M.A. Liberman, V.S. L'vov, and I. Rogachevskii, *Clustering of aerosols in atmospheric turbulent flow*, Environm. Fluid Mech. 7 (2007), pp. 173–193.
[47] J. Bec, L. Biferale, M. Cencini, A. Lanotte, S. Musacchio, and F. Toschi, *Heavy particle concentration in turbulence at dissipative and inertial scales*, Phys. Rev. Lett. 98 (2007), Article ID 084502.
[48] F. Toschi and E. Bodenschatz, *Lagrangian properties of particles in turbulence*, Annu. Rev. Fluid Mech. 41 (2009), pp. 375–404.
[49] Z. Warhaft, *Why we need experiments at high Reynolds numbers*, Fluid Dynam. Res. 41 (2009), Paper No. 021401. http://iopscience.iop.org/article/10.1088/0169-5983/41/2/021401.
[50] H. Xu and E. Bodenschatz, *Motion of inertial particles with size larger than Kolmogorov scale in turbulent flows*, Physica D 237 (2008), pp. 2095–2100.
[51] S. Balachandar and J.K. Eaton, *Turbulent dispersed multiphase flow*, Annu. Rev. Fluid Mech. 42 (2010), pp. 111–133.

[52] E.-W. Saw, G.P. Bewley, E. Bodenschatz, S. Sankar Ray, and J. Bec, *Extreme fluctuations of the relative velocities between droplets in turbulent airflow*, Phys. Fluids 26 (2014), Article ID 111702. https://doi.org/10.1063/1.4900848.
[53] T. Elperin, N. Kleeorin, M. Liberman, and I. Rogachevskii, *Tangling clustering instability for small particles in temperature stratified turbulence*, Phys. Fluids 25 (2013), Article ID 085104.
[54] T. Elperin, N. Kleeorin, B. Krasovitov, M. Kulmala, M. Liberman, I. Rogachevskii, and S. Zilitinkevich, *Acceleration of raindrop formation due to the tangling-clustering instability in a turbulent stratified atmosphere*, Phys. Rev. E 92 (2015), Article ID 013012.
[55] A. Eidelman, T. Elperin, N. Kleeorin, B. Melnik, and I. Rogachevskii, *Tangling clustering of inertial particles in stably stratified turbulence*, Phys. Rev. E 81 (2010), Article ID 056313.
[56] N. Kliorin, Y.A. Kravtsov, A. Mereminskii, and V. Mirovskii, *Clearing effects and radiative transfer in a medium with large-scale fluctuations in the density of scatterers*, Radiophys. Quantum Electronics 32 (1989), pp. 793–797.
[57] Y.A. Kravtsov, *New effects in wave propagation and scattering in random media (a mini review)*, Appl. Optics 32 (1993), pp. 2681–2691.
[58] L.A. Apresyan and Y.A. Kravtsov, *Radiation Transfer: Statistical and Wave Aspects*, Gordon and Breach, Amsterdam, 1996.
[59] E. Farbar, I.D. Boyd, and M. Esmaily-Moghadam, *Monte Carlo modeling of radiative heat transfer in particle-laden flow*, J. Quant. Spectrosc. & Rad. Trans. 184 (2016), pp. 146–160.
[60] A. Frankel, G. Iaccarino, and A. Mani, *Convergence of the Bouguer–Beer law for radiation extinction in particulate media*, J. Quant. Spectrosc. & Rad. Trans. 182 (2016), pp. 45–54. https://doi.org/10.1016/j.jqsrt.2016.05.009.
[61] Y.B. Zel'dovich and Y.P. Raizer, *Physics of Shock Waves and High-Temperature Phenomena*, Academic Press, New York, 1966.
[62] J.R. Howell, M.P. Mengüç, and R. Siegel, *Thermal Radiation Heat Transfer*, 5th ed. , CRC Press, Boca Raton, FL, 2010.
[63] M. Liberman, N. Kleeorin, I. Rogachevskii, and N.E.L. Haugen, *Mechanism of unconfined dust explosions: Turbulent clustering and radiation-induced ignition*, Phys. Rev. E 95 (2017), Article ID 051101.
[64] M. Sofiev, V. Sofieva, T. Elperin, N. Kleeorin, I. Rogachevskii, and S. Zilitinskevich, *Turbulent diffusion and turbulent thermal diffusion of aerosols in stratified atmospheric flows*, J. Geophys. Res. 114 (2009), Article ID D18209.
[65] A. Frankel, G. Iaccarino, and A. Mani, *Optical depth in particle-laden turbulent flows*, J. Quant. Spectrosc. & Rad. Trans. 201 (2017), pp. 10–16.
[66] A. Frankel, *Modeling radiation transport in turbulent particle-laden media*, Ph.D. thesis, Stanford University, August, 2017. http://purl.stanford.edu/vb385vd9358.
[67] F. Beyrau, M. Hadjipanayis, and R. Lindstedt, *Ignition of fuel/air mixtures by radiatively heated particles*, Proc. Combust. Inst. 34 (2013), pp. 2065–2072.
[68] F. Beyrau, M. Hadjipanayis, and R. Lindstedt, *Time-resolved temperature measurements for inert and reactive particles in explosive atmospheres*, Proc. Combust. Inst. 35 (2015), pp. 2067–2074.
[69] A. Acrivos and T.D. Taylor, *Heat and mass transfer from single spheres in Stokes flow*, Phys. Fluids 5 (1962), pp. 387–394.
[70] S.P. Owocki and N.J. Shaviv, *The spectral temperature of optically thick outflows with application to light echo spectra from η Carinae's giant eruption*, Mon. Not. R. Astron. Soc. 462 (2016), pp. 345–351. https://doi.org/10.1093/mnras/stw1642.
[71] J.O. Sundqvist, S.P. Owocki, D.H. Cohen, M.A. Leutenegger, and R.H. Townsend, *A generalized porosity formalism for isotropic and anisotropic effective opacity and its effects on X-ray line attenuation in clumped O star winds*, Mon. Not. R. Astron. Soc. 420 (2012), pp. 1553–1561. http://works.swarthmore.edu/fac-physics/14.